



Seismic Performance of Clay Bricks Construction

Jabbar Abdalaali Kadhim^{a*}, Abbass Oda Dawood^b

^a Postgraduate Student, Civil Engineering Department, College of Engineering, Misan University, Iraq.

^b Assist. Professor, Civil Engineering Department, College of Engineering, Misan University, Iraq.

Received 27 October 2019; Accepted 09 February 2020

Abstract

The extensive use of masonry construction accompanied by the seismic hazard in Iraq requires comprehensive studies to assess the seismic performance of such construction. This study aims to evaluate the seismic performance of URM and CM buildings by their nonlinear time-history responses. ANSYS 18.2 software has been used to perform the nonlinear dynamic analyses. The mechanical properties have been investigated as the first step of the study. A simple mechanical instrument was improvised to determine the tensile strength of masonry directly. Ground motions were chosen in a manner so that their peak ground accelerations and site soils are as similar as possible to those in the South of Iraq. The computer software terminated all the analyses before the ends of the applied earthquake duration because of the solutions did not converge. In the numerical models, severe cracks have been observed in both URM and CM models, indicating their unsafe seismic performance. The minor cracks in confining concrete in the CM model compared to the severe ones in the masonry walls of the same model show the capability of the confinement to prevent the disintegration of collapsed masonry walls, at least in damaging cases like the building state at the solution termination.

Keywords: Masonry; Confined; Earthquake; ANSYS; Cracks.

1. Introduction

Masonry is the oldest construction type used throughout the world. It was used in Mesopotamia about 5000 B.C. [1]. However, the existing Iraqi monuments denote its old usage in construction. It is still widely used in Iraq in the form of URM or CM buildings. Stones besides other building types are used in the northern and western portions of the country, while clay bricks and concrete blocks are used in the middle and southern portions. However, clay bricks masonry is mainly used in the south region. URM structures are reliable for supporting gravity loads, but their resistance is weak under the effect of lateral loads. The post-earthquake observations demonstrate how they are seismically vulnerable and how their collapse causes the majority of casualties if they represent the most buildings in the affected area. Since masonry buildings exist in regions that have effective seismicity, experimental and theoretical studies have been implemented to assess their seismic performance and to propose suitable retrofitting techniques that enhance their seismic response. In this study, the nonlinear time-history response of URM and CM buildings has been investigated by ANSYS 18.2 using the William-Waranké plasticity model to simulate the material nonlinearity. Solid65 has been used for the simulation. This element is capable of cracking in tension and crushing in compression, which is a characteristic of the mechanical behavior of brittle materials such as masonry and concrete. The element has eight nodes with three degrees of freedom at each node.

The analysis with ANSYS Mechanical APDL has three main stages: preprocessor, solution, and postprocessor. In the first stage, the model geometry is built, and the mechanical properties are input. The second stage (solution)

* Corresponding author: jabaralkhafaji1981@gmail.com

 <http://dx.doi.org/10.28991/cej-2020-03091508>



© 2020 by the authors. Licensee C.E.J, Tehran, Iran. This article is an open access article distributed under the terms and conditions of the Creative Commons Attribution (CC-BY) license (<http://creativecommons.org/licenses/by/4.0/>).

includes the definition of the boundary conditions, load application, and analysis running. In the postprocessor stage, analysis results are viewed in terms of graphs, figures, animations, or numbers. The mechanical properties of clay brick masonry have been determined through the experimental part of the study. No previous studies were found in the study area for the same purpose except the one implemented by Al-Chaar et al. [2], in which the tensile strength of masonry has not been involved in the experimental program.

The current study is not a parametric study; its primary purpose is to reveal whether the masonry models overcome the applied ground motions or not, and this is the essential criterion to evaluate their seismic performance. The mechanical properties of the numerical models should be as precise as possible. Therefore, the study headlines are the determination of masonry mechanical properties, the macro-modeling of masonry buildings, the selection of seismic waves, and applying the seismic waves to the masonry models to obtain their nonlinear time-history responses. Finally, the seismic performance of a masonry building is considered good if its model overcomes the applied ground motion. Otherwise, it is unsafe under the effect of earthquakes.

2. Literature Reviews

The structural vulnerability of masonry buildings and the dangerous effects of their damage during earthquakes lead to present many theoretical and experimental studies to assess their seismic performance and to propose suitable retrofitting techniques that enhance their structural response in 2015, Yaseen [3] investigated the seismic fragility of the URM buildings in the North of Iraq (Kurdistan region), which represent approximately 87% of all buildings in this region. The macro-modeling and the incremental dynamic analysis were performed using the TREMURI program to perform a nonlinear time-history analysis. The study indicated that the seismic safety of the studied, low-rise URM buildings in the concerned region is questionable, denoting the need for strengthening such structures to mitigate the potential economic and life losses that probably happen during future earthquakes.

Abdulla et al. (2017) [4] described a simplified micro-model for the simulation of masonry utilizing the extended finite element method and a combination of plasticity-based models. The detailed micro-modeling gives accurate and complete results, but it takes intensive computations, and thus, it is used for small masonry models. As an alternative, the researchers have proposed a simplified micro-model in which the brick units are expanded to compensate for the vanished mortar volume. Discontinuous elements model the interaction between enlarged units. The validity of the proposed method was verified by comparison to the results of experimentally tested masonry walls, which subjected to in-plane cyclic loads, out-of-plane monotonic loads, and in-plane monotonic loads. The comparison showed good accuracy for the analysis method. In 2018, Chacara et al. [5] proposed a modeling approach for unreinforced masonry structures, by which the masonry panels are simulated with quadrilateral macro-elements having rigid edges and connected by hinges and a diagonal nonlinear link. Each element has seven degrees of freedom; six degrees of freedom represent the panel translations and rotations as a rigid body, and the seventh corresponds to the shear deformation of the panel itself. The proposed modeling was performed to obtain the seismic response of two masonry models. The results of the analyses are in good agreement with those provided by finite element simulations. Also, the modeling reduces the computation cost.

Kallioras et al. (2018) [6] presented the results of an experimental test carried out on a full-scale, single-story URM building. A unidirectional-table test was implemented on the building, which is consisted of double-wythe, clay-brick URM walls including large openings and a floor made of timber beams and planks composing a flexible diaphragm. Its sharply inclined roof is composed of timber trusses. The parts of the perimeter walls above the floor (the gables) are the weaker when affected by an out-of-plane excitation. Therefore, the direction of shaking was chosen to be perpendicular to these walls. It was observed that only minor damage occurred for the affected building up to an input accelerogram with a PGA (peak ground acceleration) of 0.23 g, while the collapse state was reached at motion with a PGA of 0.68 g. Zones of high acceleration response, such as gables, exhibited major out-of-plane damage. As a result, the study confirmed that the most vulnerable parts of such buildings under seismic action are the gable walls, while the rocking of slender piers exhibited the damage caused by the in-plane response. In 2018, Avila L. et al. [7] assessed the seismic performance of two prototypes of asymmetric masonry buildings. One of the buildings is a two-story, unreinforced building, while the other is a two-story, reinforced building. The study involved investigating the effect of geometrical configuration, the influence of reinforcement presence, and the comparison between the seismic behaviors of the two structures. It has been found that the reinforced building is capable of inputting acceleration twice the acceleration that input to the unreinforced building. Shakarmi et al. (2018) [8] used the LS-DYNA software for the simulation of confined masonry walls loaded with cyclic, in-plane, lateral loads to examine the effect of aspect and reinforcement ratio on the structural behavior of the studied walls. The validity of using the micro-model has been verified by comparing it to the results of a previous test performed on a confined wall. The study showed that an aspect ratio of (height/length=1) makes the wall having better structural behavior concerning resisting mechanism, energy absorption, and deformability.

Erberik et al. (2019) [9] compared the seismic performance of URM buildings to that of CM buildings. The results demonstrated the superior, seismic performance of CM buildings over URM ones. It was found that low rise CM

buildings are suitable, even high seismic intensity exists. The confinement enhances the seismic behavior by preventing wall-to-wall action that propagates seismic damage and also to the enhancement of the structural capability of dissipating energy. The results demonstrated a high effect of masonry compressive strength on the seismic performance of URM buildings. Whereas, it is not the case for CM building models, which are notably affected by other parameters such as the reinforcement and the cross-section of confining concrete columns and diagonal shear strength of confined masonry walls. In 2019, Cazarin and Teran-Gilmore [10] discussed the relatedness of some of the new seismic provisions of the code known as “the Mexico City Building Code” released in December 2017, which increases the deformation demand of the inter-storey drift from 0.5% to 1% for CM buildings with shear walls having horizontal reinforcement. Three CM buildings of different numbers of stories (6, 8, and 10 stories) were designed according to the code requirements. Then the non-linear static analyses were performed to obtain the responses of the three buildings. The experimental evidence for the justification of the increase in lateral displacement was studied. For the three buildings, it was found that a soft story is developed in the building once its maximum shear capacity is reached. Beyond that, failure occurs if a minimal increase occurs in the lateral displacement. It was observed that a drift of 1% could not be reached before the development of the soft storey. In 2019, Dong et al. [11] presented an experimental study to investigate the effect of reinforced mortar cross strips on the structural response of unreinforced masonry walls subjected to seismic loadings. Eight walls strengthened with cross strips of reinforced mortar on one or both faces, and three URM walls were tested under the effect of a lateral cyclic load with constant pressure on the top face. It was found that the presence of reinforced mortar cross strips increased the shear strength by at least 38.2% and significantly increased the deformation capacity.

Ismail and Khattack (2019) [12] studied failure modes of the URM buildings that were damaged due to the Mw 7.5 earthquake that hit the North of Pakistan on 26 October 2015. The commonly observed failure modes encompassed toppling of minarets, local or global out-of-plane collapse of URM walls, diagonal shear cracking in piers, flexural cracking in spandrels, damage of corner, pounding damage, and damage due to ground settlement. Most fatalities were due to the collapse of URM walls and subsequent collapse of roofs. In 2019, Sorrentino et al. [13] studied the structural behavior of masonry buildings during the nine earthquakes ranging from 5 to 6 of the moment magnitude that hit Central Italy during the period between August 2016 and January 2017. The unreinforced masonry buildings represent about 75% of the constructions in the affected territory. Severe damage and complete collapse were observed in URM buildings, while better structural behavior was observed in modern buildings constructed with hollow clay blocks. This better seismic performance is attributed to the adequate quality of masonry, the relatively lightweight structures due to the presence of cavities in masonry units and the configuration redundancy.

3. Mechanical Properties of Masonry

3.1. Compressive Strength

The compressive strength of masonry can be considered its fundamental characteristic because the other mechanical properties can be estimated depending on it by proposed relationships. Masonry compressive strength depends on the compressive strength of its constituents (brick units and mortar). The difference in stiffness and Poisson's ratio between bricks and mortar makes one of the two constituents expands laterally more than the other as masonry being compressed. Consequently, shear stresses develop at the contact surfaces between bricks and mortar initiating masonry failure [14]. If the bricks are stiffer than mortar, the mortar will be in a triaxial compression state of stress. Meanwhile, the cannon will be stretched outside if it is more inflexible. In the present study, six masonry prisms were tested, as in Figure 1, and the average compressive strength is 5.5 MPa with a standard deviation of 0.4 MPa.



Figure 1. A prism specimen under test

3.2. Tensile Strength

The tensile strength of each of the masonry constituents is higher than the ultimate value of the bond stress exhibited perpendicular to their interaction surface. Therefore, the tensile strength of masonry is controlled by the ultimate value of this stress. In the present study, a simple method was used to test the tensile strength of masonry directly. The specimen used for the test is two bricks built together, as in Figure 2, with cement-sand mortar of 1:3 mixing proportion.

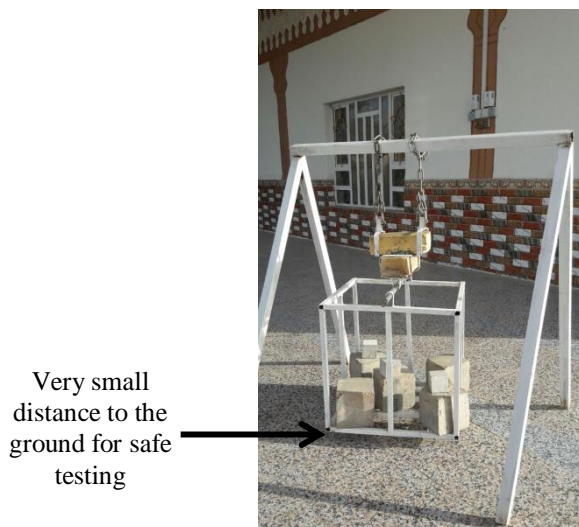


Figure 2. Tensile strength test of masonry

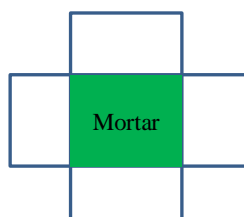


Figure 3. A sketch for the top view of a specimen of masonry tensile test

The lower brick of the specimen, shown in Figure 2, is loaded by the hanging weights that are put in the lower iron frame, which is free to fall when the tensile failure occurs, while the upper brick remains hanging at the top. Bricks, sand, concrete cubes, etc. are put in the suspended frame up to failure occurs. Then, all weights, including iron frame and lower brick, are summed and divided by the loaded area, which is the intersection area illustrated in Figure 3. The result of the division represents the tensile strength of the masonry specimen. Fifteen specimens were tested in this study, and the average value of the tensile strength is 0.15 MPa with a standard deviation of 0.03 MPa.

3.3. Modulus of Elasticity

The modulus of elasticity of masonry (E_m) can be estimated by the compressive strength value, but the challenge is that the codes have a large extent of variation in the recommended relationships as shown in Table 1.

Table 1. Different Formulae for evaluating modulus of elasticity of masonry

Code	Recommended value for masonry modulus of elasticity in MPa
Building Code Requirements and Specifications for Masonry Structures by the Masonry Standards Joint Committee (MSJC) [15]	$700f_m$ or evaluated as the slope of the chord taken between 0.05 and 0.33 of the compressive strength of masonry in the stress-strain curve
Eurocode 6 [16]	$1000 f_m$
FEMA 356 [17]	$550 f_m$

Where f_m : Compressive strength of masonry in MPa.

In the present study, a simple steel frame was prepared to measure the modulus of elasticity. Three prisms (three-brick prisms) were tested under uniaxial compression, as shown in Figure 4b. The length shortening was measured

with a dial gauge, and the corresponding load was recorded. Only the eight screws (two from each side) touch the specimen, as in Figure 4a.

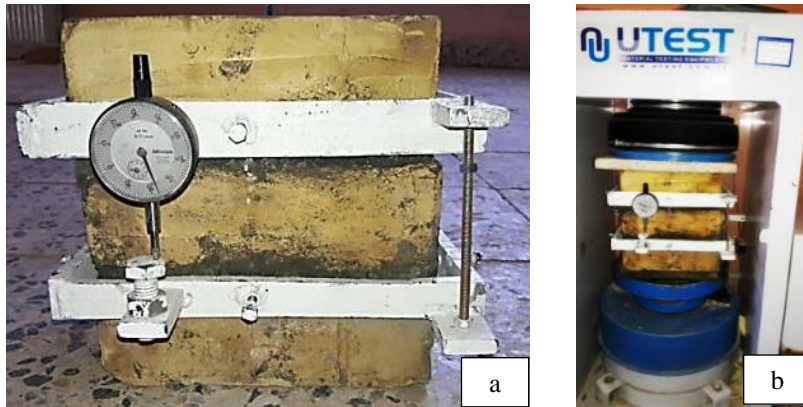


Figure 4. (a) A Specimen with apparatus; (b) A specimen under testing

The modulus of elasticity can be obtained from the stress-strain curve according to the MSJC code [15], as illustrated in Figure 5, in which the modulus of elasticity is the slope of the line segment joining the two points on the curve whose stresses are 0.33 and 0.05 f_m , where f_m is the compressive strength of masonry. Consequently, the moduli of elasticity for the three specimens have been evaluated from the stress-strain curves shown in Figures 6 to 9 as in Table 2.

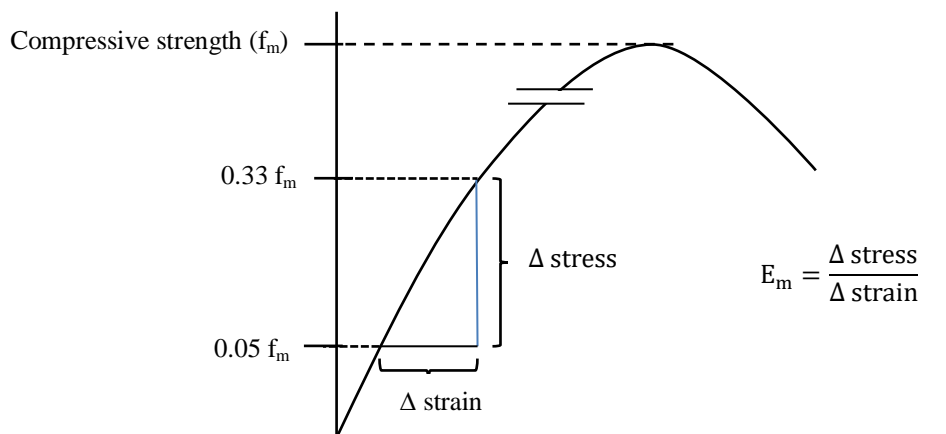


Figure 5. Modulus of elasticity for masonry according to MSJC code [15]

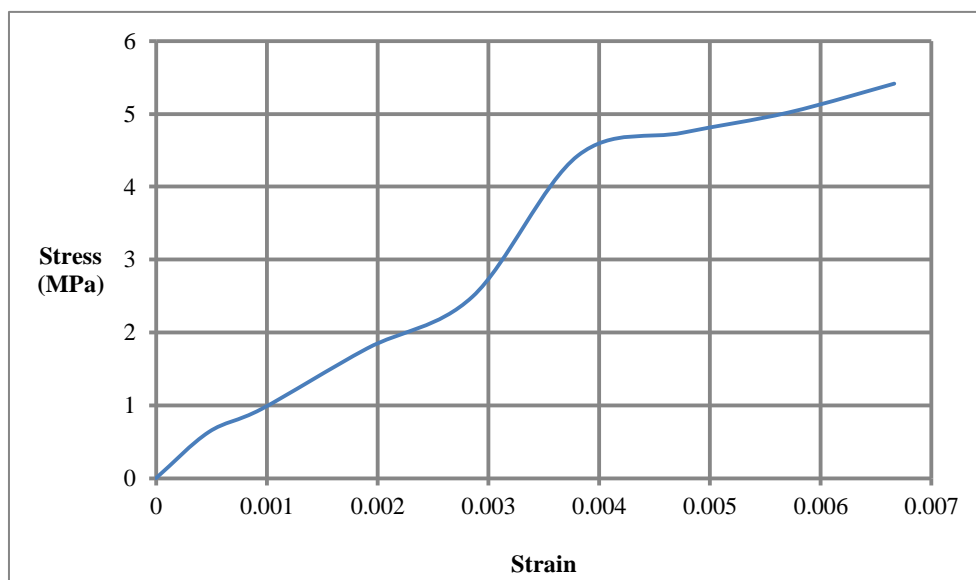


Figure 6. Stress-Strain curve for masonry specimen No.1

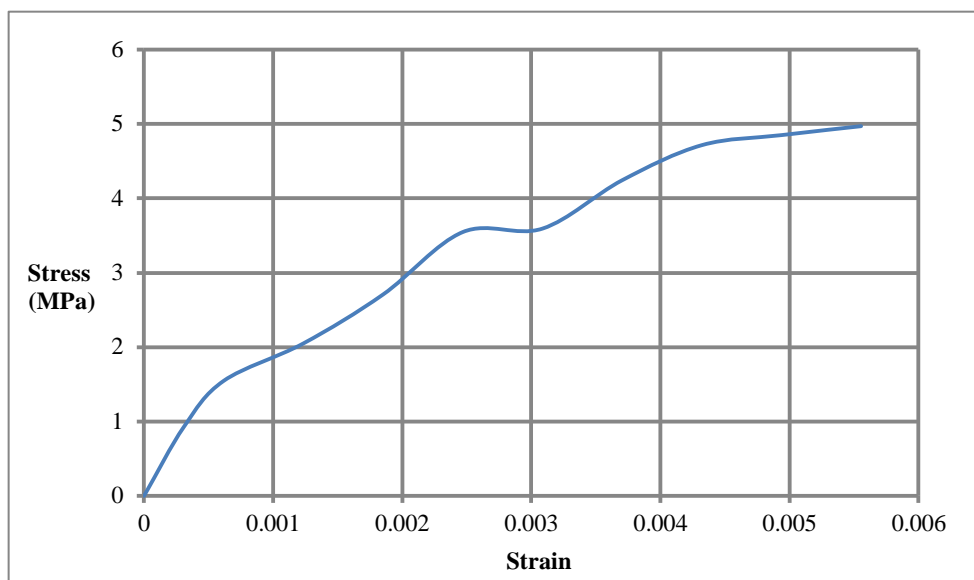


Figure 7. Stress-Strain curve for masonry specimen No.2

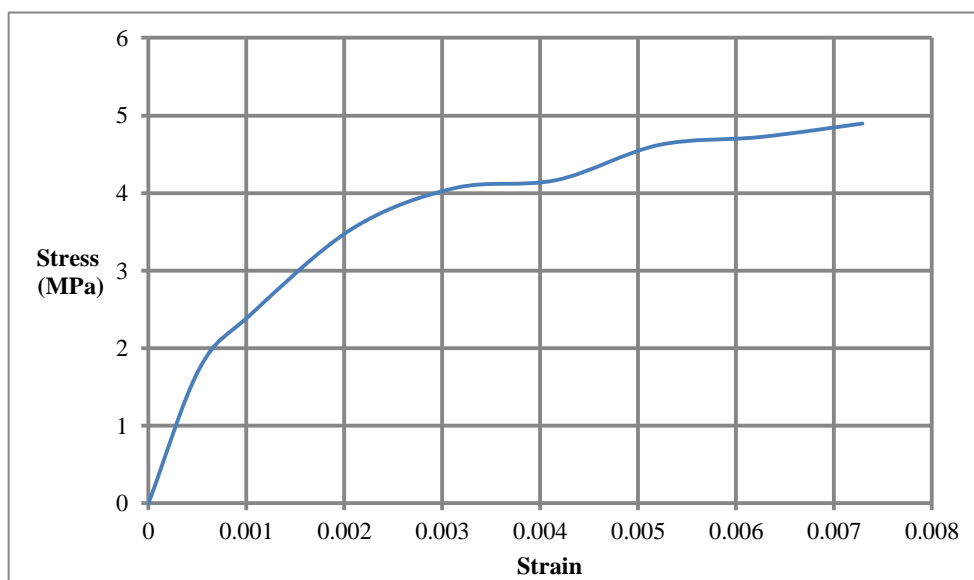


Figure 8. Stress-Strain curve for masonry specimen No.3

Table 2. Moduli of elasticity of masonry specimens

No. of masonry specimen	Modulus of elasticity (MPa)
1	2399
2	3610
3	2160

The average value of modulus of elasticity is 2723 MPa with a standard deviation of 777 MPa. The significant variation between the results is due to the difference between brick units, which have pretest cracks with different configurations. However, a value of 2750 MPa for the modulus of elasticity has been used in the analyses.

4. Transient Analysis

The transient analysis (also called time-history) is one of the analysis types provided by ANSYS software. It is used to determine the response of a linear or a nonlinear structural system subjected to any time-dependent load. Also, it can be used to find the response of a freely vibrating structure with or without damping effect. In this analysis type, ANSYS solves the overall equilibrium equations in the form below [18]:

$$[M]\{\ddot{U}\} + [C]\{\dot{U}\} + [K]\{U\} = \{F_t\} \tag{1}$$

Where: $[M]$ is the global mass matrix, $\{\ddot{U}\}$ is the vector of nodal accelerations, $[C]$ is damping matrix, $\{\dot{U}\}$ is the vector of nodal velocities, $[K]$ is the global stiffness matrix, $\{U\}$ is the vector of nodal displacements, and $\{F_t\}$ is the load vector.

At any time (t), the set of equations above can be considered as equations of static equilibrium, and the program utilizes the iterative approach to solve them. For the sequent time increments, an improved method (known as HHT) or Newmark integration method is used to perform the incremental dynamic analysis [20].

5. Seismic Loading for Transient Analysis

The seismic load is defined into ANSYS mechanical APDL to perform a transient analysis by applying the ground velocity and displacement that is traveled by the structure foundation during the earthquake to the nodes or areas at the level of structure base. An acceleration time-history can be converted into a displacement time-history by the double integration technique, which is nowadays carried out by professional software packages such as Seismosignal software. In the present study, seismic data files were downloaded from the site of the PEER Berkeley ground motion database. Also, the acceleration time-histories of the 7.3 Mw earthquakes that hit the Iraq-Iran border on 12 November 2017 were converted to displacement time-histories and used in the analysis. The ground acceleration files for the mentioned earthquake were downloaded from the site of the Iranian strong motion database.

6. Selection of Acceleration Time-Histories

The ground motions that chosen for the structural analysis should be as reflective as possible for the seismic characteristics of the analyzed structures site. In this study, the criteria used to select the seismic records are the magnitude (Mw), the peak ground acceleration (PGA), and the average shear wave velocity for the upper 30 m from the site soil (vs30). The statistical analysis for Iraq seismicity reveals that 90.05% of events have magnitudes within the range (4-5.4), while 6.03% of the total events have magnitudes within the range (5.5-7.4). The contour map of the peak ground acceleration, according to the PSHA study introduced by Onur et al. [19], is shown in Figure 9. In the South of Iraq, the PGA map shows that its value increases from 0.1g to more than 0.5g as the site varies towards the Iraq-Iran borderline. Therefore, the selected ground accelerations have PGAs within this range.

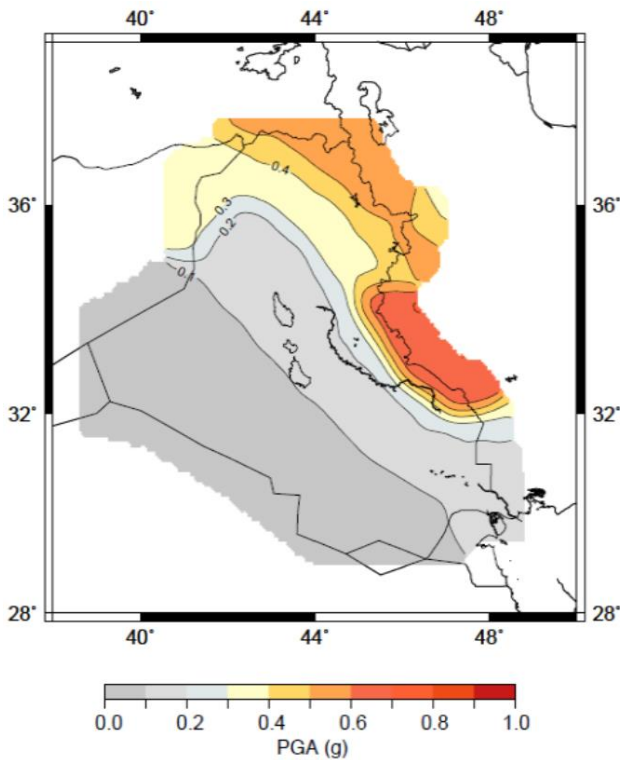


Figure 9. Peak ground acceleration map for Iraq [19]

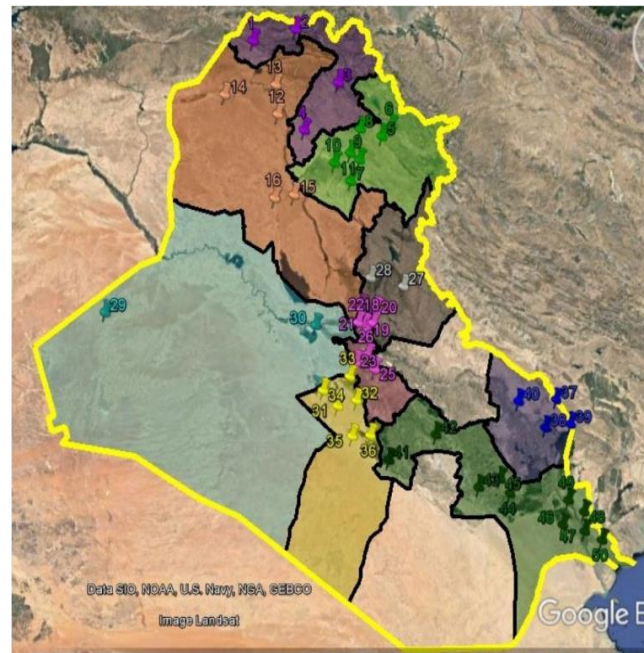


Figure 10. Distribution of projects used by Mohammed and Abdurassol [20]

The shear wave velocity (v_{s30}) for an area can be estimated depending on the reported site investigations that were performed for projects erected in it. In 2017, Mohammed and Abdurassol [20] evaluated the shear wave velocity for different sites in Iraq, depending on the geotechnical reports of the projects distributed, as in Figure 10. The main parameter used in the study is the standard penetration test (SPT), which can be used as an alternative parameter to classify sites instead of the shear wave velocity. The study evaluated the shear wave velocity ranging from 102 to 627 m/s in the South of Iraq and from 111 to 420 m/s in the Eastern South. The low values of the ranges are for soft clay soil, which is obviously observed in Basra city.

7. Modeling and Results

7.1. Model No. 1

The model is a one-story, single room with a plan shown in Figure 11 and a clear height of 3 m. It has two openings; the (1×2.1) m door and the (1×1.5) m window. The concrete slab thickness is 0.2 m. The wall thickness is 0.24 m. The lintels over openings are made of concrete. The finite element model is shown in Figure 12.

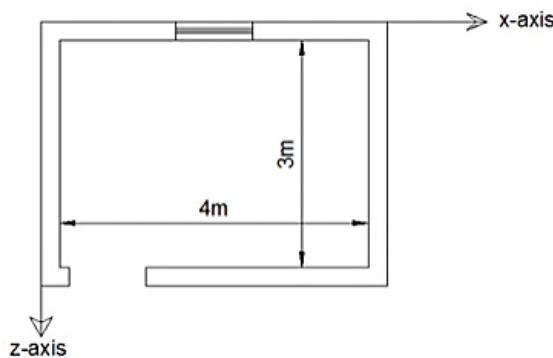


Figure 11. plan of Model No.1

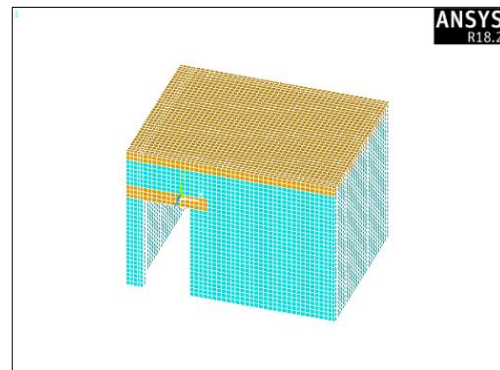


Figure 12. Finite element model No.1

The coordinate system, shown in Figure 11 is the same as the default global coordinate system in ANSYS in which the y-axis is perpendicular to the paper (parallel to the room height). The edge length of the element was set to be 100 mm. Thus, the model is built up of 16164 solid65 elements with 22548 nodes. The characteristics of the seismic records applied to the model are as in Table 3.

Table 3. Description of the seismic records applied to model No.1

Earthquake name	Station name	Date	Magnitude (M_w)	Peak ground acceleration (g)	Shear velocity (v_{s30}) (m/s)
Northwest California	Ferndale city hall	12/9/1938	5.5	0.15	219.31

The acceleration time-histories for the earthquake mentioned above are shown in Figures 13 to 15.

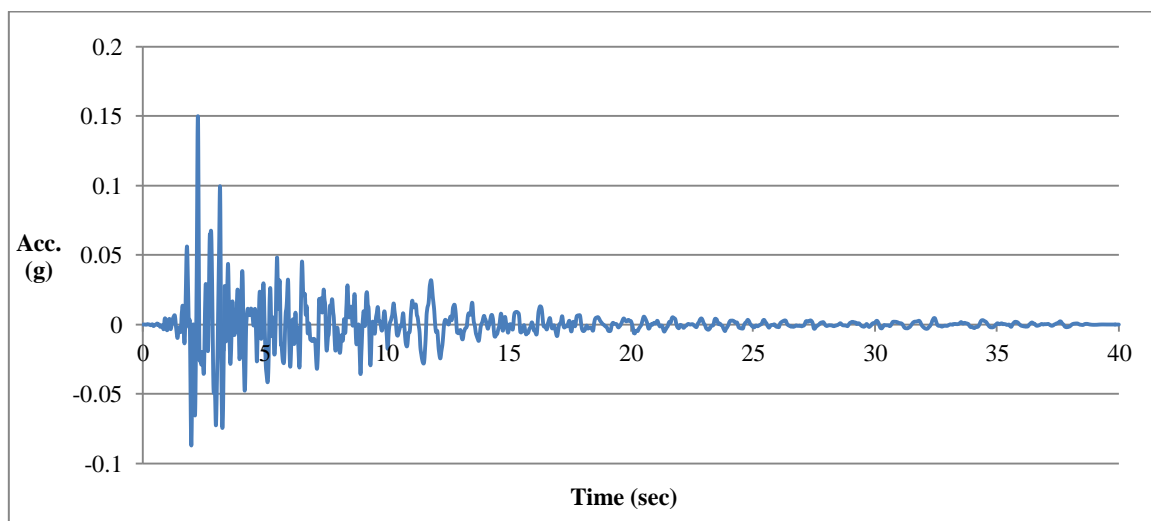


Figure 13. H-1 component of ground acceleration of Northwest California earthquake, 1932

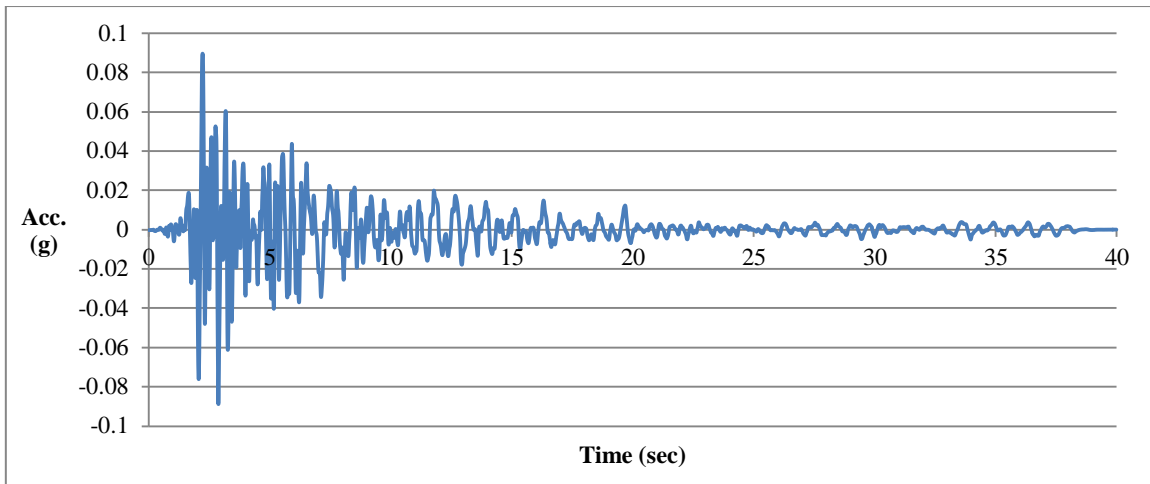


Figure 14. H-2 component of ground acceleration of Northwest California earthquake, 1932

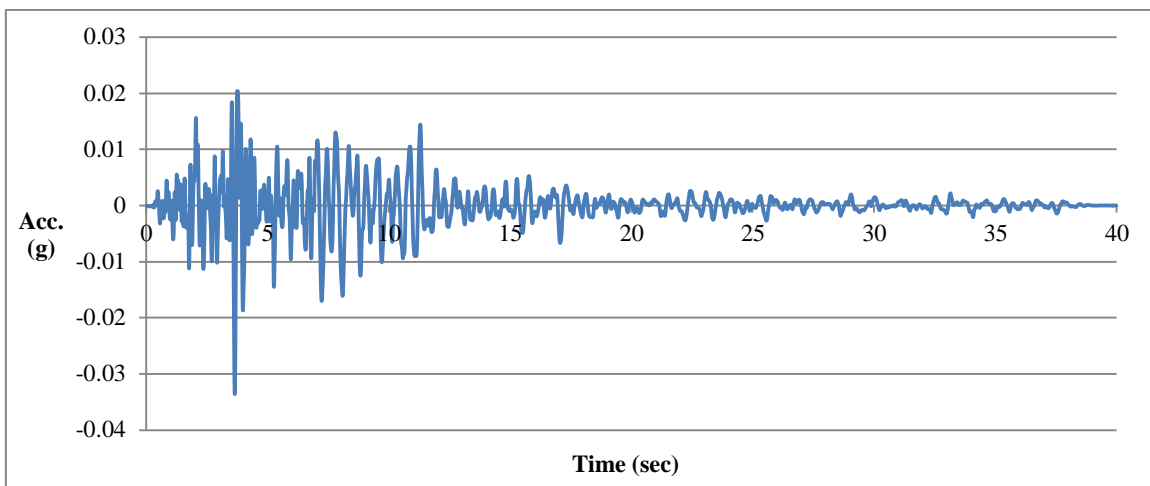


Figure 15. Vertical component of ground acceleration of Northwest California earthquake, 1932

The horizontal H-1 components of ground velocity and displacement were applied in the z-direction, while the horizontal H-2 and vertical components were applied in the x-, and y-direction (gravity direction), respectively. The solution did not converge and terminated at a time of 0.7 seconds. The total displacement in the z-direction at roof level is shown in Figure 16.

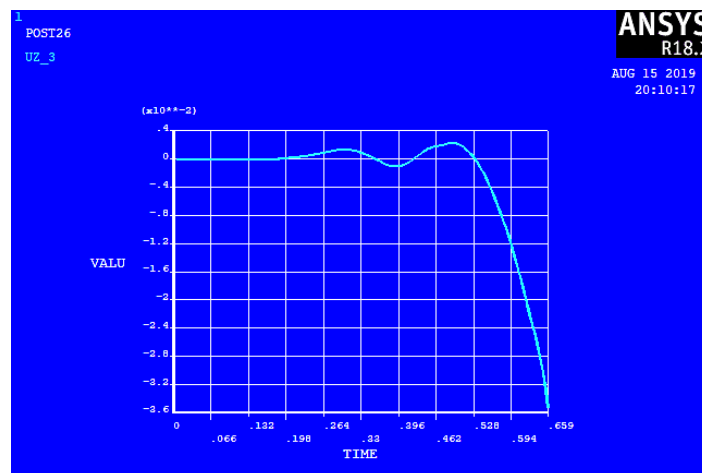


Figure 16. Total displacement at roof level in z-direction for Model No.1 in mm

It is so important to know that the displacement, given in ANSYS postprocessor at any node, is the total displacement (u^t) at that node. Therefore, the differential (deformation) displacement (u) between any two nodes (any two points within the structure) is found from subtracting ANSYS displacements for the two nodes one from the other. The total displacement (u^t) is given by Equation 2.

$$u^t = u_g + u \tag{2}$$

Where: u^t is the total displacement, u_g is the ground displacement, and u is the response (deformation). Figure 17 shows the three displacements in the sketch below:

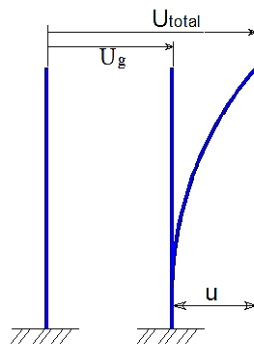


Figure 17. Displacement nomenclature

The ANSYS displacement (total displacement) at the base level is the same as the ground displacement since the structure base is assumed in full integrity with the ground. Therefore, the response (displacement) in the z-direction at the roof level has been found with the use of the Excel software by subtracting the ANSYS displacement at base level in the z-direction from the ANSYS displacement at roof level in the same direction. Figures 18 and 19 show the ANSYS displacement at the base level and the response at the roof level (uz), respectively.

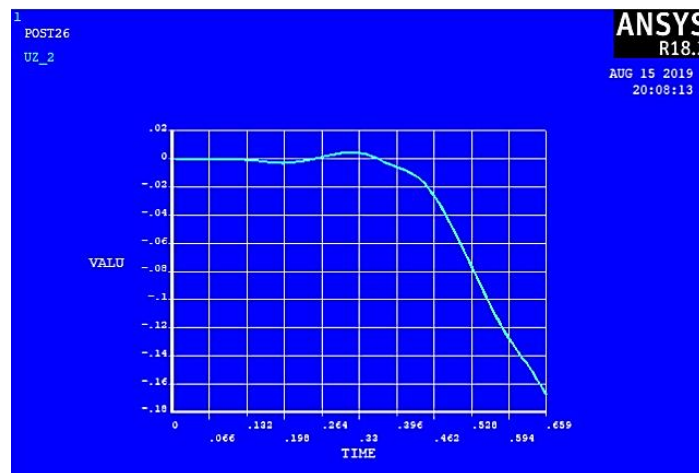


Figure 18. Total displacement at base level in z-direction for Model No.1 in mm

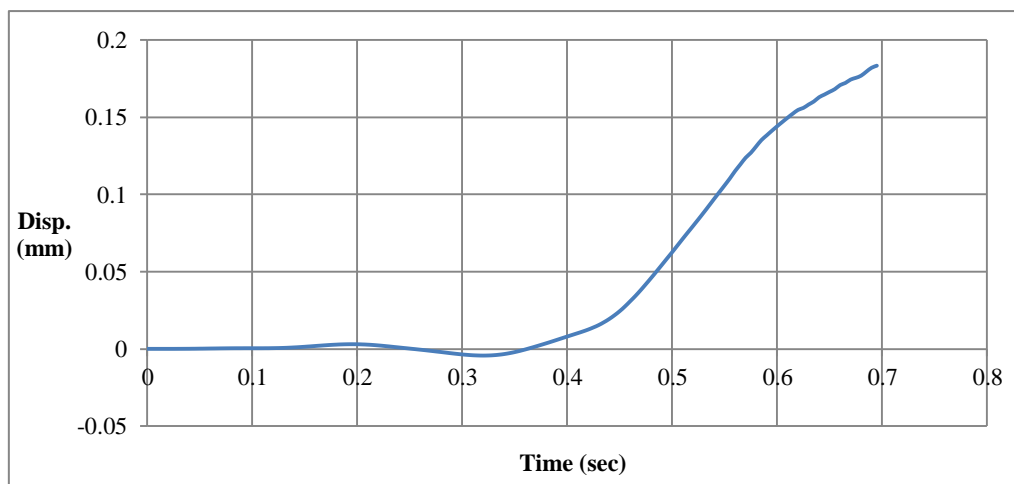


Figure 19. The response at roof level in z-direction for Model No.1

Similarly, subtracting the ANSYS displacement at the base level in the x-direction from the ANSYS displacement at the roof level in the same direction by using Excel resulted in the response in x-direction shown in Figure 20.

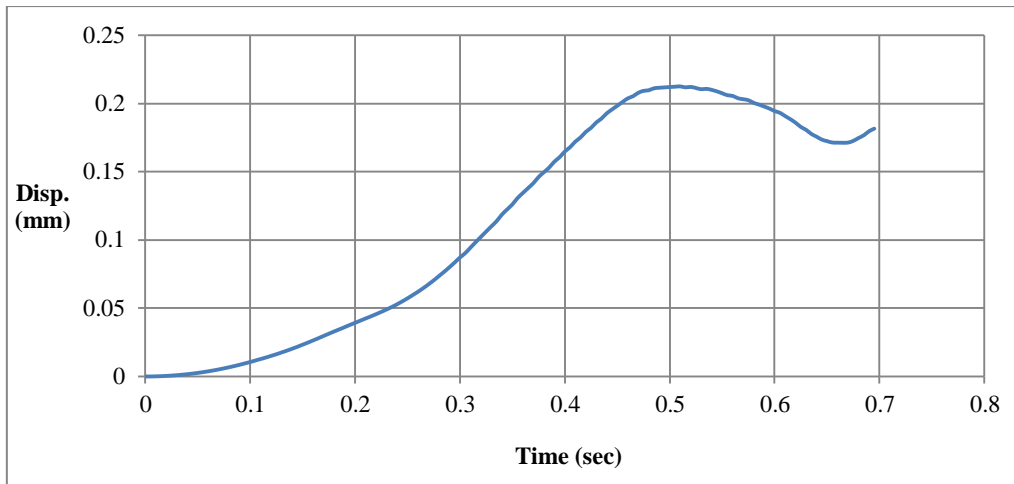


Figure 20. The response at roof level in x-direction for Model No.1

The end of the solution is as shown in Figure 21, in which the diagonal cracks and horizontal cracks at the bottom courses can be clearly observed. The cracks are colored with red color, and the blue color refers to the locations where the first cracks occur which has appeared near the corners of the door and the window in Model No.1 as shown below:

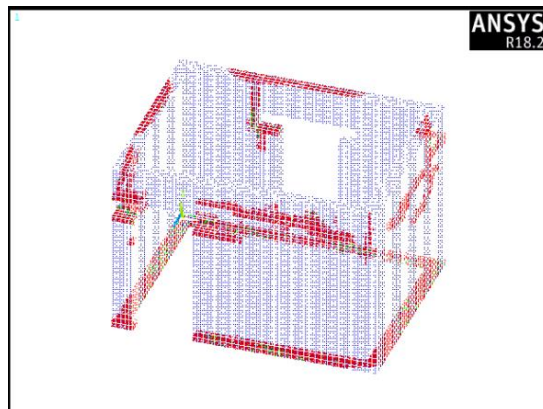


Figure 21. Cracks in walls of Model No.1 at the end of the solution

7.2. Model No.2

The model is a one-story typical house with a clear height of 3 m and a plan shown in Figure 22.

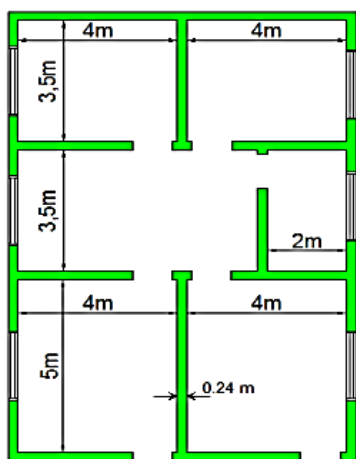


Figure 22. Plan of the typical house

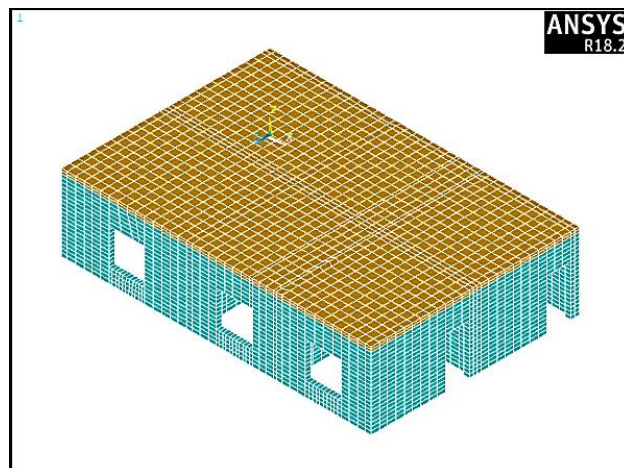


Figure 23. Finite element model No.2

The roof is a concrete slab having 0.2 m thickness. The finite element model is shown in Figure 23, in which the edge length of the element was set to be 200 mm, thus the model is built up of 4289 solid65 elements with 8868 nodes. The displacement-time histories used for the analysis were obtained from converting the accelerograms recorded in Ravansar station (Iranian station) during the 7.3 Mw earthquakes that hit the Iraq-Iran border on 12 November 2017. The accelerograms were converted to displacement time-histories by the use of seismosignal software. Table 4 demonstrates the characteristics of the seismic records applied to Model No.2.

Table 4. Description of the seismic records applied to Model No.2

Earthquake name	Station name	Date	Magnitude (M_w)	Peak ground acceleration (g)	Shear velocity (VS30) (m/s)
The 7.3 Mw, November 2017	Ravansar	12/11/2017	7.3	0.122	267

The acceleration time-histories for the earthquake mentioned above are shown in Figures 24 to 26.

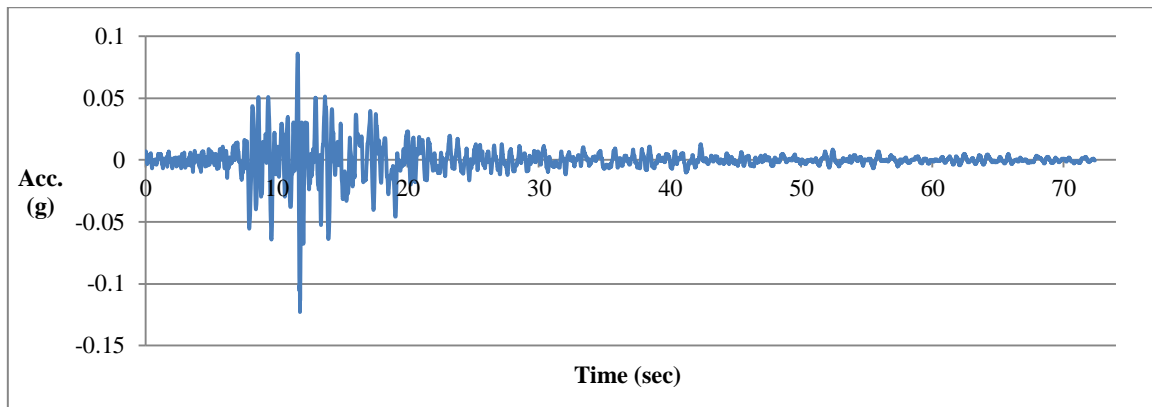


Figure 24. H-1 component of ground acceleration of the 7.3 Mw, November 2017 earthquake

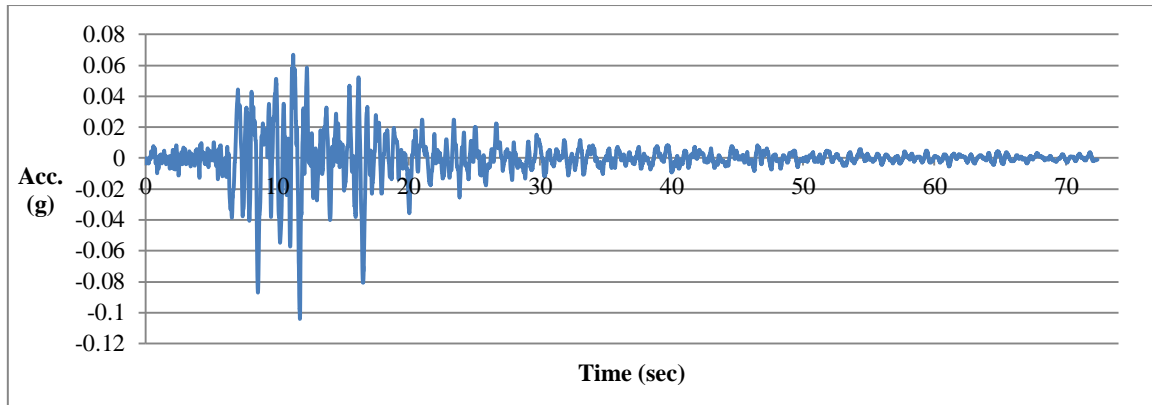


Figure 25. H-2 component of ground acceleration of the 7.3 Mw, November 2017 earthquake

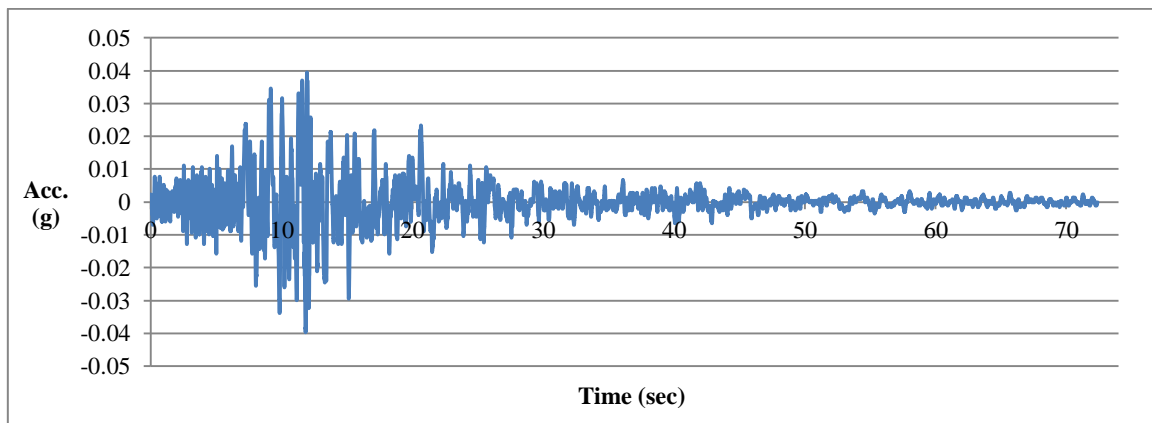


Figure 26. Vertical component of ground acceleration of the 7.3 Mw, November 2017 earthquake

The horizontal H-1 components of ground velocity and displacement were applied in the z-direction, while the second horizontal H-2 components were used in the x-direction. Of course, the vertical components were applied in gravity direction (y-direction). The structure responses in z and x directions are shown in Figures 27 and 28, respectively.

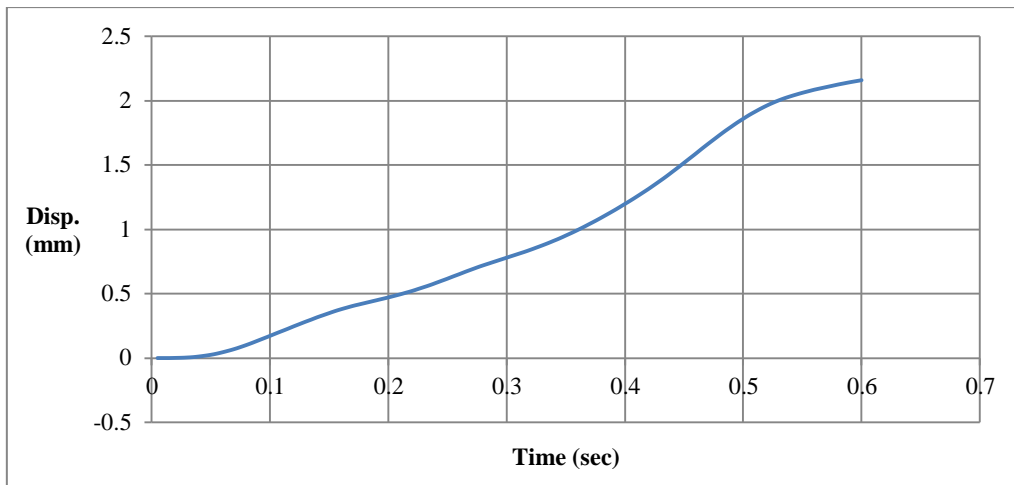


Figure 27. Response at roof level in z-direction for Model No.2

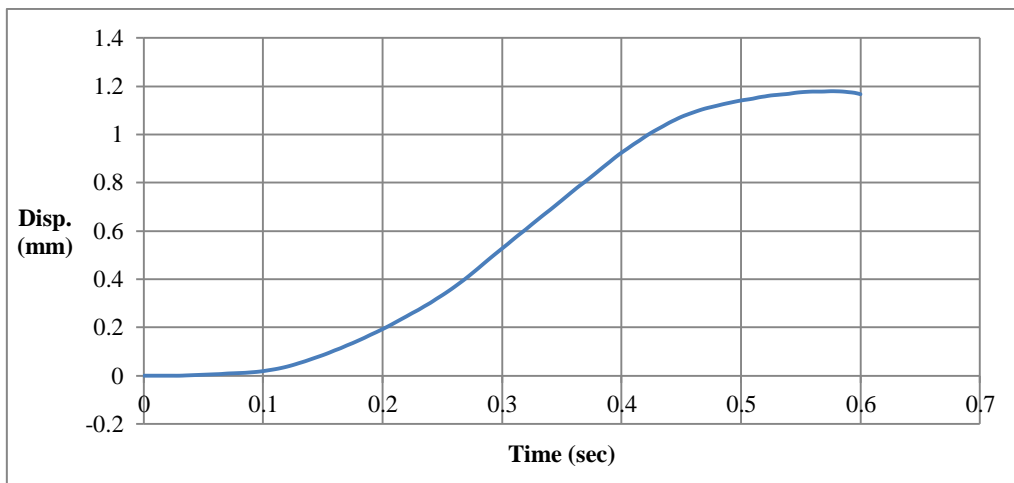


Figure 28. Response at roof level in x-direction for Model No.2

The crack pattern in the masonry walls of Model No.2 at the end of the solution is shown in Figure 29.

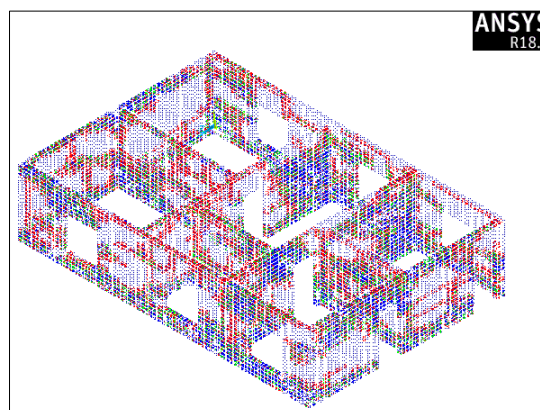


Figure 29. Crack pattern in masonry walls of Model No.2 at end of solution

No cracks were observed in the concrete slab, as can be seen in Figure 30 which shows the crack pattern in the slab.

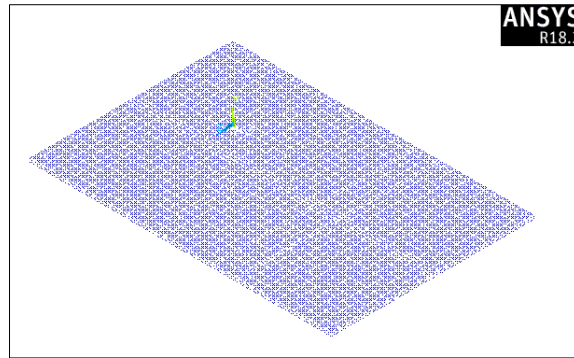


Figure 30. Crack pattern in concrete slab of Model No.2 at end of solution

The mesh was refined to check the acceptance of the element size, and thus the length of the element edge was set to be 150 mm. The analysis was repeated. The responses of the roof level in z-direction before and after mesh refinement are as shown in Figure 31. It can be noticed that a negligible variance occurred in the structure response. Therefore, the element size with a 200 mm edge length is acceptable.

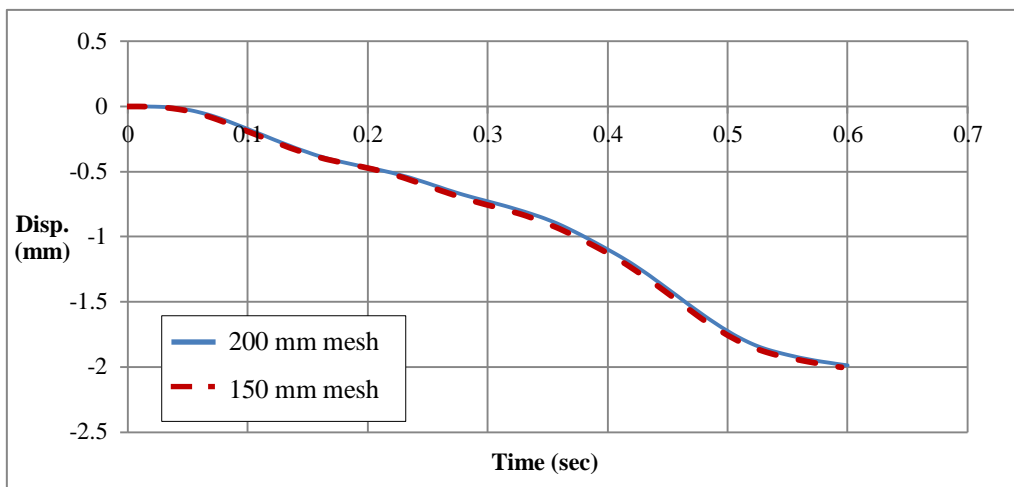


Figure 31. Responses at roof level in z-direction before and after mesh refinement for Model 2

7.3. Model No.3

This model is a two-story building with a repeated plan of a single room shown in Figure 32. The size of the element is 200 mm, and thus the finite element model shown in Figure 33 is built up of 5780 solid65 elements with 9261 nodes.

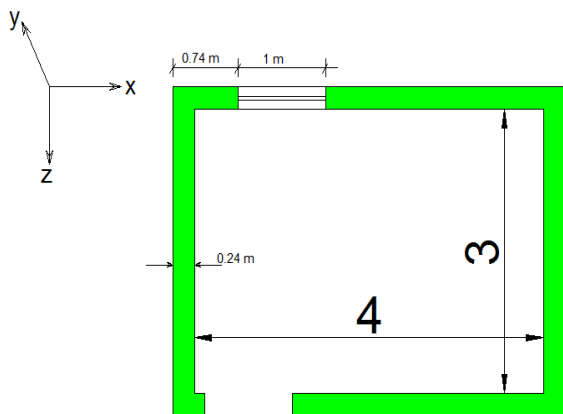


Figure 32. Plan of Model No.3

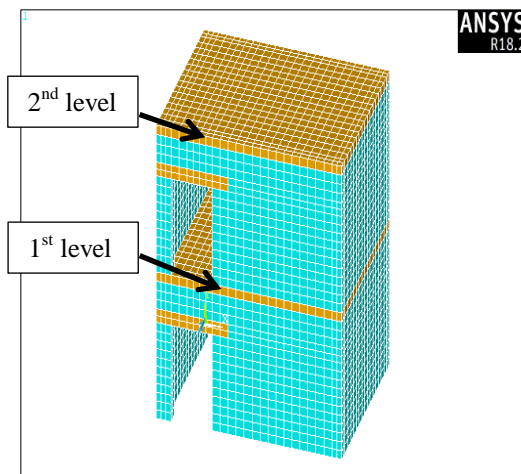


Figure 33. Finite element Model No.3

The seismic loading is the same loading applied to Model No.1. The responses at first and second levels are shown in Figures 34 to 37.

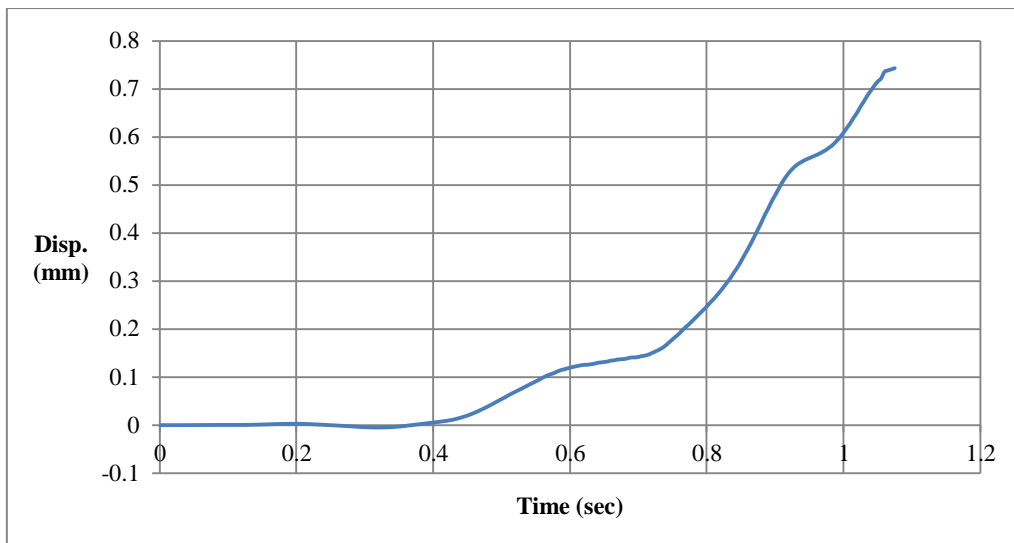


Figure 34. Response at first level in z-direction for Model No.3

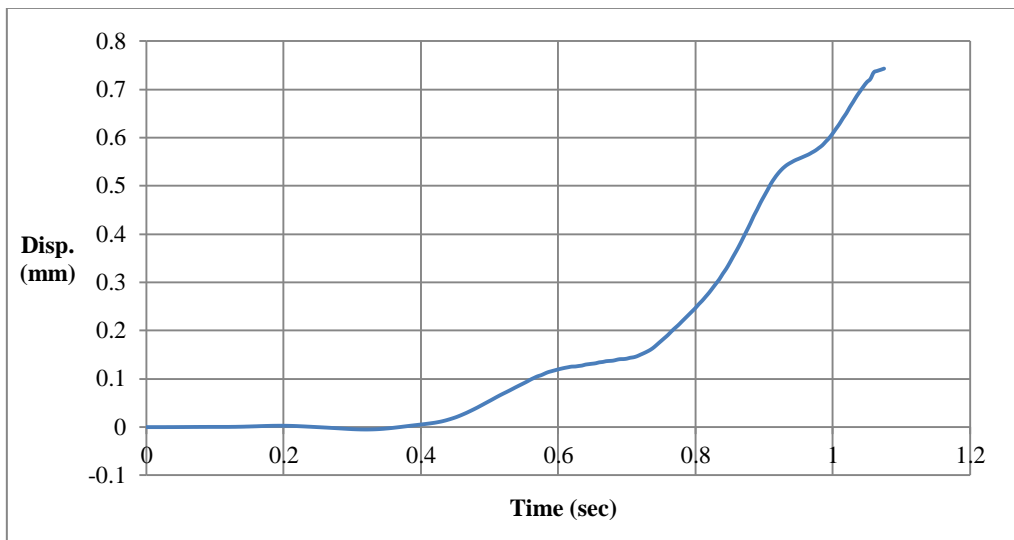


Figure 35. Response at second level in z-direction for Model No.3

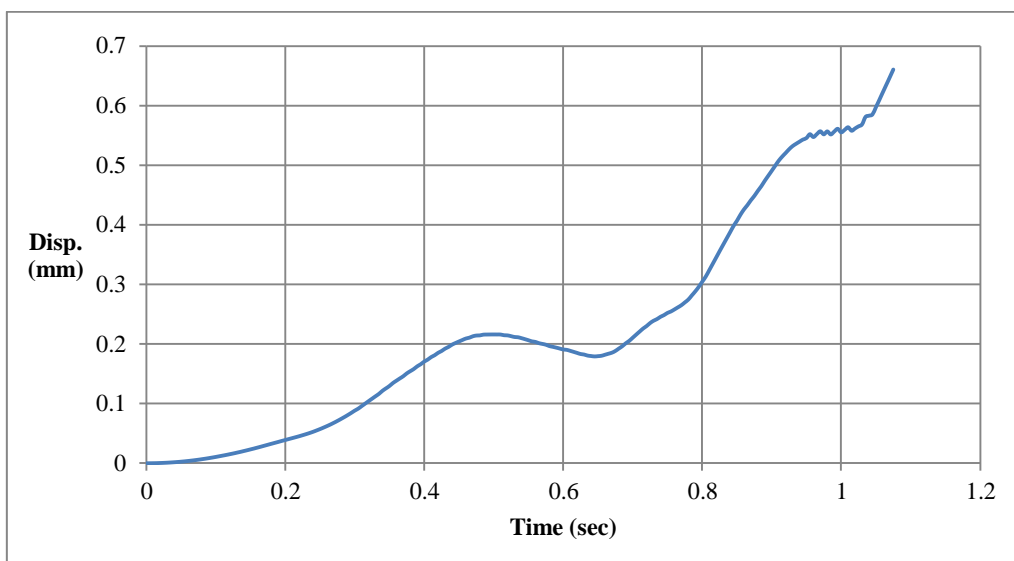


Figure 36. Response at first level in x-direction for Model No.3

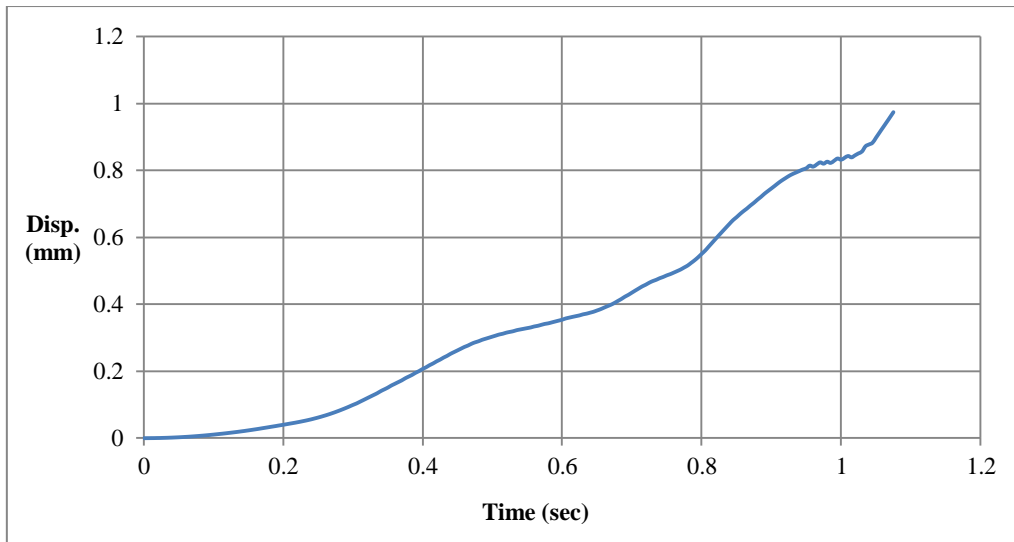


Figure 37. Response at second level in x-direction for Model No.3

Figure 38 shows locations of the building where first cracks appear in masonry walls while Figure 39 shows crack pattern at the end of the solution.

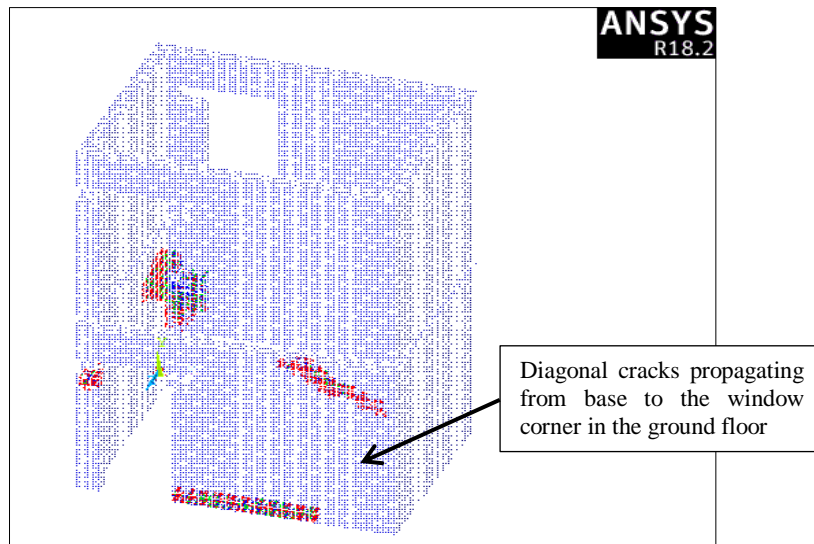


Figure 38. First cracks in masonry walls of Model No.3

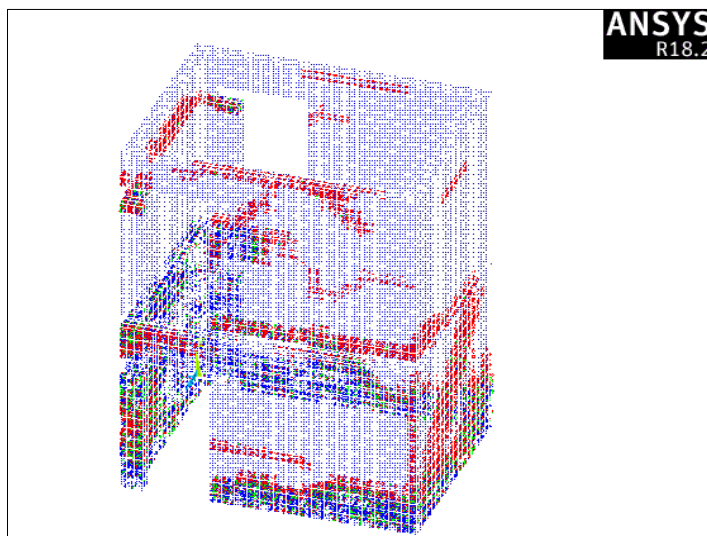


Figure 39. Crack pattern in masonry walls of Model No.3 at end of solution

7.4. Model No.4

The model is a confined, single-story, masonry room having the same plan and dimensions as those of Model No.1. The vertical confining components (tie-columns) have a cross-section of (240×240) mm. They are reinforced with 4 Ø12 mm longitudinal bars and Ø6 mm @200 mm ties. The mechanical properties of concrete and reinforcement steel are as in Table 5.

Table 5. Mechanical properties of concrete and reinforcement steel

Material	Compressive Strength (MPa)	Tensile strength (MPa)	Modulus of Elasticity (MPa)	Poisson's ratio
Concrete	25	3.5	24000	0.2
Reinforcement steel	---	400	200,000	0.3

The finite element model, shown in Figure 40, is composed of 32728 solid65 elements and 6637 beam elements with 39072 nodes. The finite element simulation of columns reinforcement is shown in Figure 41. The seismic loading is the same loading used in Model No.1.

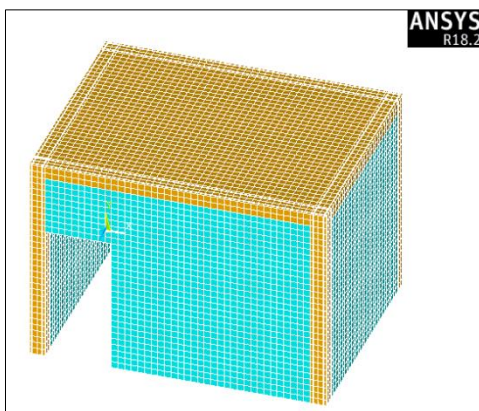


Figure 40. Finite element Model No.4

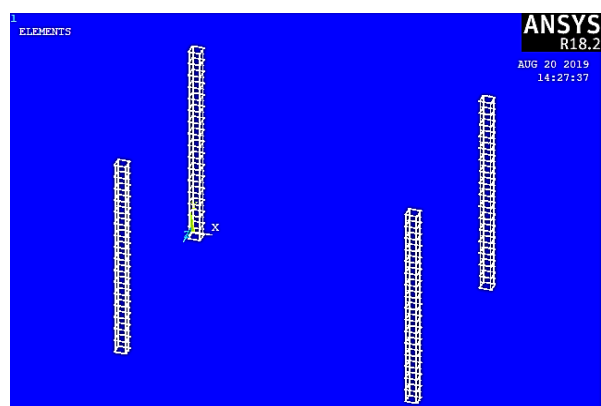


Figure 41. Simulation of columns reinforcement in Model No.4

The responses at roof level in z and x directions are shown in Figures 42 and 43.

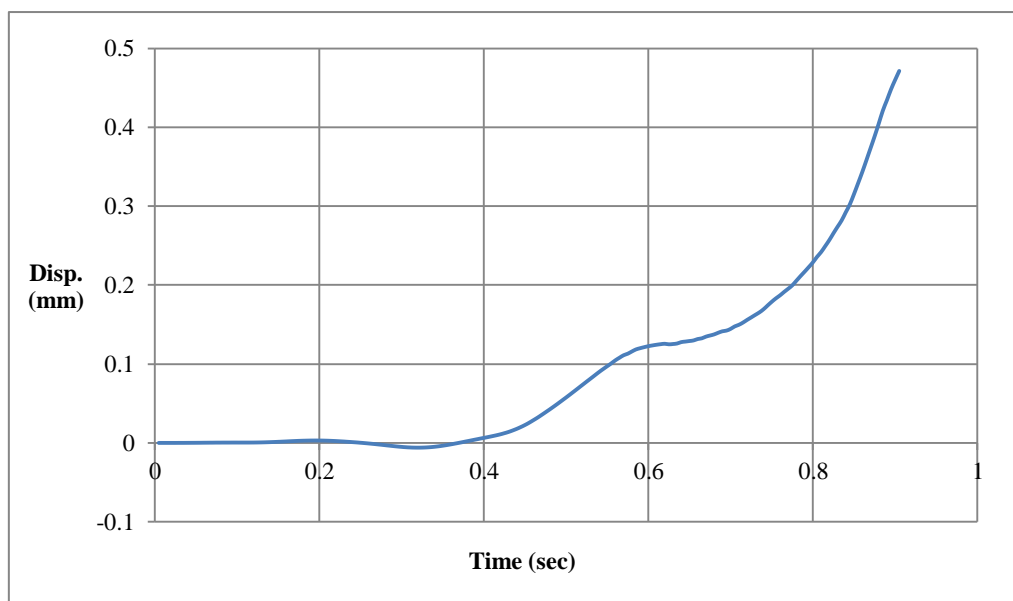


Figure 42. Response at roof level in z-direction for Model No.4

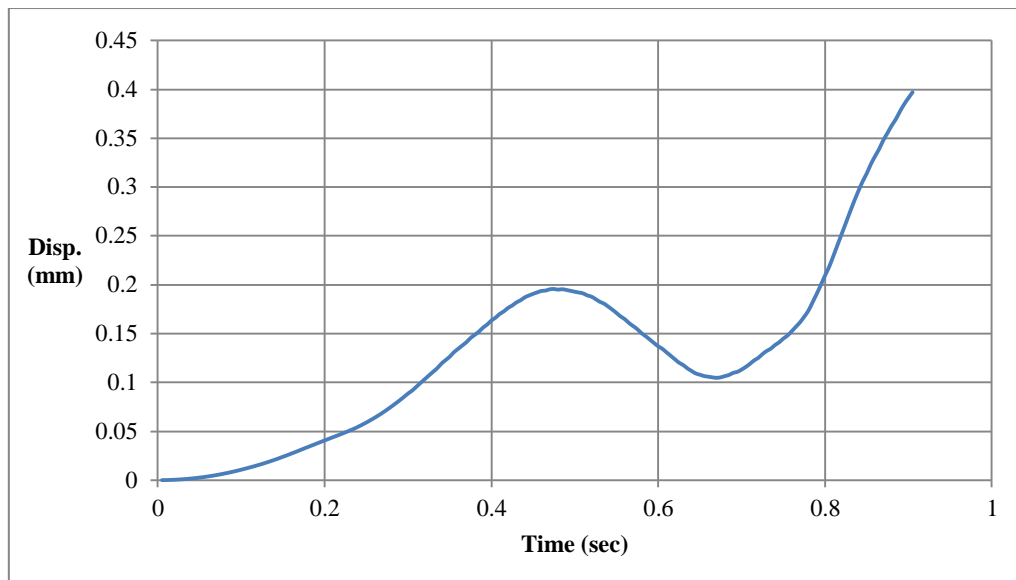


Figure 43. Response at roof level in x-direction for Model No.4

Figures 44 and 45 show the crack pattern in masonry walls and concrete frame (slab and confining tie columns):

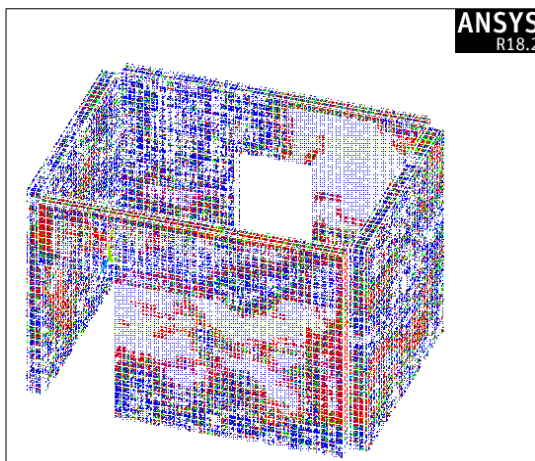


Figure 44. Crack pattern in walls of Model No.4

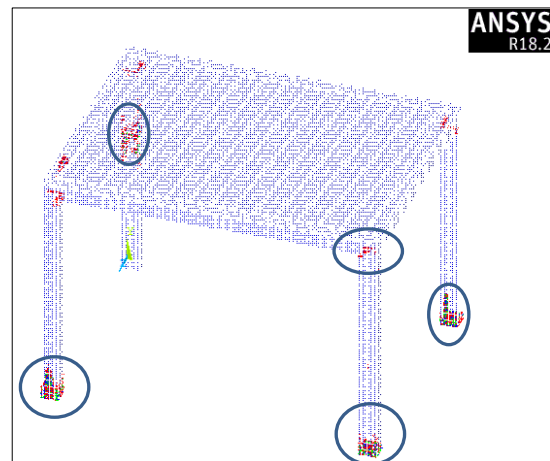


Figure 45. Crack pattern in the concrete frame of Model No.4

The stress in the reinforcement of the tie-columns is shown in Figure 46. The maximum stress value is 191.684 MPa which is less than one half the yield stress of the reinforcement.



Figure 46. Stress in steel reinforcement of confining columns in Model No.4

8. Results and Discussion

The solution of nonlinear equations, in which the stiffness matrix is a function of the degrees of freedom or their derivatives, is accomplished in ANSYS using the Newton-Raphson method. The Newton-Raphson equation used for the nonlinear solution can be written as in Equation 3 that follows [18]:

$$[K_i^T] \cdot \{\Delta U_i\} = \{F^a\} - \{F_i^{nr}\} \quad (3)$$

Where: $[K_i^T]$ is the tangential stiffness matrix, $\{\Delta U_i\}$ is the displacement increments, $\{F^a\}$ is the applied loads vector, and $\{F_i^{nr}\}$ is the vector of element internal loads. In transient analysis, $\{F_i^{nr}\}$ includes the effective inertia and damping forces. The present study ignored the damping effect. The set of the simultaneous equations in the form of Equation 3 are solved with an iterative process. The iterative process requires a convergence criterion to terminate when the solution satisfies the required accuracy. The nonlinear convergence criteria are used in ANSYS for the nonlinear structural solutions which are solved by the Newton-Raphson method. Force, displacement, moment, and rotation criteria are provided. In the present study, both force and displacement criteria were used.

The main criterion adopted in the study to assess the seismic performance of a studied structure is whether it resists and overcomes the applied seismic waves or not. All simulated buildings could not overcome the applied seismic loadings. Here, it should be interpreted, according to Equation 3, what it means if the convergence is not satisfied. It means that the right-hand side of the equation does not equal the left-hand side within the limited tolerance. This inequality is attributed to the reduction in the stiffness matrix, which is caused by the missing stiffness of cracked elements. Consequently, the structure no longer has the required stiffness to resist the applied forces.

The dynamic responses shown in Figures 19, 20, 27, 28 and 34 to 37 demonstrate the combined effect of in-plane and out-of-plane actions since the diaphragm (concrete slab) has two orthogonal, horizontal displacements in z and x directions. It can be observed that all studied models oscillated a few cycles, not about their equilibrium positions. The combination of responses and crack patterns arouses the inquiry of how these significant cracks occur with small deformations. The answer to this inquiry requires the determination of yield displacement of URM masonry walls in terms of the parameters governing it. In 2010, Aldemir [21] introduced a parametric study to determine the parameters affecting the structural behavior of unreinforced masonry piers subjected to lateral, in-plane loads. Then, the study has formulated the parameters of the capacity curve of URM walls. According to the mentioned study, the yield displacement of URM walls is given in Equation 4.

$$\delta_y = 0.587 p^{0.543} \cdot e^{0.0949 f_m} \cdot \lambda^{1.426} \cdot L \quad (4)$$

Where: δ_y , p , e , f_m , λ , and L are: yield displacement in mm, overburden pressure in MPa, the natural exponent, compressive strength of masonry in MPa, aspect ratio, and the length of the wall in mm, respectively. The overburden pressure on the top of the masonry wall has an essential effect on its structural behavior. Therefore, the gravity load profoundly affects the stability of URM structures subjected to lateral loads. ANSYS software applies the loads incrementally during the solution time, which is the earthquake duration in the transient analysis of seismic response. Consequently, only a part of the concrete slab is applied at the top faces of walls before the solution termination. For more accuracy, this problem must be taken into consideration to overcome. Taking Model No.1 as an example with an overburden pressure of 0.03 MPa, the yield displacement in the z-direction is 0.41 mm. Comparing this calculated value to the response shown in Figure 19 reveals that the two masonry walls in z-direction yielded with deformations less than those estimated by Equation 4. However, Equation 4 has been formulated depending on a statistical process, and is not very strict. The pressure of 0.03 MPa is the bearing stress on top faces of masonry walls parallel to the short dimension due to the weight of the concrete slab, which is the pressure in a static case. As explained above, the incremental application of loads means that the overburden pressure at the end of the solution is much less than 0.03 MPa since the solution terminated at a very early moment during the earthquake duration. Besides, Equation 4 has been formulated for a static case with an in-plane action only, which differs from the dynamic behavior. Finally, cracking of in-plane loaded URM walls with small deformations agrees with the results of previous studies. Increasing the tolerance for the nonlinear convergence criteria, which has a default value of 0.001, through the solution controls input makes the solution continue more time leading to more significant deformations in the analyzed structure. However, using high tolerances in solutions needs shaking table tests to make comparisons between the experimental results and the numerical results to verify the validation of the high values. Therefore, future studies must consider this need.

9. Conclusion

It is not strict enough to say that the studied models collapsed or not, during the applied seismic waves because the analyses stopped before the occurrence of the total collapse, which cannot be captured obviously by ANSYS simulations. However, the three URM models that studied could not overcome the applied earthquakes, and significant cracks occurred in them. Consequently, it is right to consider the unreinforced masonry buildings as unsafe structures

under the effect of a seismic load due to their poor seismic performance. All models cracked with small deformations. Therefore, the nonlinear, dynamic analysis appears more conservative than the nonlinear, static analysis (pushover analysis). The crack patterns show that the first cracks appear near openings in masonry walls, and cracking occurs firstly on the ground floor in case of a two-story building.

To some extent, the locations of first cracks verify the accuracy of the simulation results because it is already clear that the stresses concentrate near openings, and the maximum shear force occurs at the base of the building during earthquakes if the fundamental mode governs its dynamic behavior. However, the first crack locations reveal the need for strengthening the openings of doors and windows with a suitable confinement technique. The confined masonry model also was not capable of overcoming the applied earthquake, but the minor cracks in the tie-columns compared to the significant cracks in masonry walls and unyielding of reinforcement show a good indication that the confinement can preserve the collapsed masonry walls from disintegration, which reduces losses in life and properties. Based on the study results, no guided conclusion can be presented about the structural behavior of the confined masonry building beyond the time of the end of the solution, but it is overbalanced that spreading of cracks in the concrete frame continues in progress while a detachment of brick units mainly happens in the out-of-plane direction.

10. Acknowledgement

The authors would like to thank the dean of college of engineering and all the lecturers of civil engineering department in Misan University.

11. Conflicts of Interest

The authors declare no conflict of interest.

12. References

- [1] Zimmermann, Thomas, and Alfred Strauss. "Masonry and Earthquakes: Material properties, Experimental testing and Design approaches." *Earthquake-Resistant Structures: Design, Assessment and Rehabilitation* (2012): 177.
- [2] Al-Chaar, Ghassan K., Steven C. Sweeney, Jonathan C. Trovillion, Orange S. Marshall, and Brendan Danielson. *Pseudo Dynamic Testing and Seismic Rehabilitation of Iraqi Brick, Bearing and Shear Walls*. No. ERDC/CERL-TR-08-6. Army Engineer District Los Angeles CA, 2008.
- [3] Yaseen, Abdulhameed Abdullah. "Seismic Fragility Assessment of Masonry Buildings in the Kurdistan Region." PhD diss., University of Portsmouth, 2015.
- [4] Abdulla, Kurdo F., Lee S. Cunningham, and Martin Gillie. "Simulating Masonry Wall Behaviour Using a Simplified Micro-Model Approach." *Engineering Structures* 151 (November 2017): 349–365. doi:10.1016/j.engstruct.2017.08.021.
- [5] Chácará, César, Francesco Cannizzaro, Bartolomeo Pantò, Ivo Caliò, and Paulo B. Lourenço. "Assessment of the Dynamic Response of Unreinforced Masonry Structures Using a Macroelement Modeling Approach." *Earthquake Engineering & Structural Dynamics* (July 6, 2018). doi:10.1002/eqe.3091.
- [6] Kallioras, Stylianos, Gabriele Guerrini, Umberto Tomassetti, Beatrice Marchesi, Andrea Penna, Francesco Graziotti, and Guido Magenes. "Experimental Seismic Performance of a Full-Scale Unreinforced Clay-Masonry Building with Flexible Timber Diaphragms." *Engineering Structures* 161 (April 2018): 231–249. doi:10.1016/j.engstruct.2018.02.016.
- [7] Avila, Leonardo, Graça Vasconcelos, and Paulo B. Lourenço. "Experimental Seismic Performance Assessment of Asymmetric Masonry Buildings." *Engineering Structures* 155 (January 2018): 298–314. doi:10.1016/j.engstruct.2017.10.059.
- [8] Shakarami, B., M. Z. Kabir, and R. Sistani Nezhad. "Parametric Study on Confined Masonry Walls Subjected to In-plane Cyclic Loading Through Numerical Modeling." *AUT Journal of Civil Engineering* 2, no. 1 (2018): 49-58. doi: 10.22060/ajce.2018.12560.5257.
- [9] Erberik, Murat Altug, Cihan Citiloglu, and Gulden Erkoseoglu. "Seismic Performance Assessment of Confined Masonry Construction at Component and Structure Levels." *Bulletin of Earthquake Engineering* 17, no. 2 (September 8, 2018): 867–889. doi:10.1007/s10518-018-0468-8.
- [10] Cazarin E.F.E. and A. Teran-Glimore. "Seismic Performance of Confined Masonry Buildings Designed with the Mexico City Building Code. The thirteen North American Masonry Conference." June 16-19, 2019. Salt Lake City, UT, USA. Available online: <https://www.researchgate.net/publication/333907513>.
- [11] Dong, Sui, Jiang, and Zhou. "Experimental Study on Seismic Behavior of Masonry Walls Strengthened by Reinforced Mortar Cross Strips." *Sustainability* 11, no. 18 (September 5, 2019): 4866. doi:10.3390/su11184866.

- [12] Ismail, Najif, and Nouman Khattak. "Observed Failure Modes of Unreinforced Masonry Buildings During the 2015 Hindu Kush Earthquake." *Earthquake Engineering and Engineering Vibration* 18, no. 2 (April 2019): 301–314. doi:10.1007/s11803-019-0505-x.
- [13] Sorrentino, Luigi, Serena Cattari, Francesca da Porto, Guido Magenes, and Andrea Penna. "Seismic Behaviour of Ordinary Masonry Buildings During the 2016 Central Italy Earthquakes." *Bulletin of Earthquake Engineering* 17, no. 10 (April 24, 2018): 5583–5607. doi:10.1007/s10518-018-0370-4.
- [14] Kaushik, Hemant B., Durgesh C. Rai, and Sudhir K. Jain. "Stress-strain characteristics of clay brick masonry under uniaxial compression." *Journal of materials in Civil Engineering* 19, no. 9 (2007): 728-739. doi:10.1061/(ASCE)0899-1561(2007)19:9(728).
- [15] M. S. J. Committee, "Building Code Requirements and Specification for Masonry Structures: Containing Building Code Requirements for Masonry Structures (TMS 402-11/ACI 530-11/ASCE 5-11)." *Specification for Masonry Structures (TMS 602-11/ACI 530.1-11/ASCE 6-11)*.
- [16] British Standard. "Eurocode 6: Design of masonry structures." British Standard Institution. London (2005).
- [17] A. S. o. C. Engineers, "Prestandard and Commentary for The Seismic Rehabilitation of Buildings." FEMA, 2000. Available online: <https://www.nehrp.gov/pdf/fema356.pdf>.
- [18] Kohnke, Peter. "ANSYS Mechanical APDL Theory Reference." Canonsburg, PA, USA: ANSYS Inc (2013).
- [19] Onur, Tuna, Rengin Gok, Wathiq Abdalnaby, Ammar M. Shakir, Hanan Mahdi, Nazar M.S. Numan, Haydar Al-Shukri, Hussein K. Chlaib, Taher H. Ameen, and Najah A. Abd. "Probabilistic Seismic Hazard Assessment for Iraq" (May 6, 2016). doi:10.2172/1305883.
- [20] Mohammed, Qassun Sa'ad Al-Deen, and Murtadha A. Abdurassol. "Database of dynamic soil properties for most Iraq soils." *American Scientific Research Journal for Engineering, Technology, and Sciences (ASRJETS)* 37, no. 1 (2017): 230-254.
- [21] A. Aldemir, "A Simple Seismic Performance Assessment Technique for Unreinforced Brick Masonry Structures." Master's Thesis, Middle East Technical University Civil Engineering Department, Ankara, Turkey, 2010.